ELSEVIER

# In$_3$Ir$_3$B, In$_3$Rh$_3$B and In$_5$Ir$_9$B$_4$, the first indium platinum metal borides

## Wilhelm Klünter, Walter Jung*

*Institut für Anorganische Chemie, Universität zu Köln, Greinstr. 6, D-50939 Köln, Germany*

## Abstract

The first indium platinum metal borides have been synthesized and structurally characterized by single crystal X-ray diffraction data. In$_3$Ir$_3$B and In$_3$Rh$_3$B are isotypic. They crystallize with the hexagonal space group $P\bar{6}2m$ and $Z = 1$. The lattice constants are $a = 685.78(1)$ pm, $c = 287.30(1)$ pm for In$_3$Ir$_3$B and $a = 678.47(3)$ pm, $c = 288.61(6)$ pm for In$_3$Rh$_3$B. The structure which is derived from the Fe$_2$P type is characterized by columns of boron centered triangular platinum metal prisms inserted in a three-dimensional indium matrix. The indium atoms are on split positions. In$_5$Ir$_9$B$_4$ (hexagonal, space group $P\bar{6}2m$, $a = 559.0(2)$ pm, $c = 1032.6(3)$ pm, $Z = 1$) crystallizes with a structure derived from the CeCo$_3$B$_2$ type. The structure can be interpreted as a layer as well as a channel structure. In part the indium atoms are arranged at the vertices of a honeycomb net (Schlaefli symbol 6$^3$) separating slabs consisting of double layers of triangular Ir$_6$B prisms, and in part they form a linear chain in a hexagonal channel formed by iridium prisms and indium atoms of the honeycomb lattice.

© 2006 Elsevier Inc. All rights reserved.

## 1. Introduction

Of the ternary transition metal borides with a group IIIa metal as the third component, only those with aluminum have been studied to a larger extent. Many of these compounds crystallize with simple structures built up by only two structure elements: a boron centered triangular transition metal prism and a more or less distorted transition metal cube centered by an aluminum atom. Examples are AlMn$_2$B$_2$ [1], AlFe$_2$B$_2$ [2,3], AlCr$_2$B$_2$ [4], Al$_2$Ru$_3$B$_2$, Al$_3$Ru$_4$B$_2$ [5], Al$_5$Ru$_9$B$_6$ [6], Al$_3$Os$_4$B$_2$ and Al$_2$Fe$_3$B$_2$ [7].

Only a few compounds with the congeners gallium and indium have been described till now, and no thallium transition metal borides are known. The structures of GaRu$_2$B$_2$ and Ga$_2$Ru$_3$B$_2$ [7] correspond to those of the majority of aluminum compounds cited above with gallium atoms in distorted cubes formed by ruthenium atoms and boron atoms in triangular ruthenium prisms. Ga$_3$Pt$_9$B$_4$ and Ga$_2.7$Ir$_9$B$_4$ [8] crystallize with channel structures in which the gallium atoms in the channels have coordination number 9 + 2. Furthermore $\tau$-phases with gallium [9–11] and the gallium-rich compound Ga$_8$Ir$_4$B [12] have been reported. With indium only four ternary phases are known: the $\tau$-phases In$_2$Co$_{21}$B$_6$ [13] and In$_2$Ni$_{21}$B$_6$ [14] and the perovskite analogous InSc$_3$B [15] and InNi$_{3.5}$B$_{0.5}$ [16]. Both structure types are very flexible and can adopt a great variety of elements. In order to learn more about the specific role of indium in the crystal chemistry of ternary borides, we began with a systematic study on ternary indium transition metal borides. In the course of this investation we synthesized the first indium platinum metal borides. Here we report on the isotypic compounds In$_3$Ir$_3$B and In$_3$Rh$_3$B and on In$_5$Ir$_9$B$_4$. The compounds In$_{6/7}$Ir$_4$B$_3$, In$_{6/7}$Ir$_6$B$_4$, and In$_3$Pt$_4$B will be the subject of forthcoming papers.

## 2. Experimental procedures

### 2.1. Syntheses and chemical properties

Starting materials for the syntheses were indium powder (99.99%, Ventron), iridium- and rhodium-powder (99.9%,

---

*Corresponding author. Fax: +49 221 470 5083.
  *E-mail address:* walter.jung@uni-koeln.de (W. Jung).

Degussa) and boron-powder prepared from boron pieces (99.8%, Aldrich) in a boron carbide mortar.

Pristine $In_3Ir_3B$ was obtained by reaction of an appropriate mixture of the elemental components in an alumina crucible sealed in a silica ampoule under argon atmosphere. In a first step the mixture was heated at a rate of $100\,°C/h$ to a temperature of $1100\,°C$, which was maintained for 50 h. The reaction product was homogenized in a boron carbide mortar, heated to $1000\,°C$ for 50 h and cooled down to room temperature at a rate of $10\,°C/h$.

In the case of $In_3Rh_3B$ the same procedure was used. However, a small amount of InRh was formed as a by-product. If boron was applied in excess of 50%, no by-products could be observed in the X-ray powder pattern, but most probably excessive boron, not visible in the powder pattern, remains in the sample.

$In_5Ir_9B_4$ was prepared by arc-melting a compacted mixture of the elemental components in the appropriate composition from both sides on a water-cooled copper plate under argon atmosphere using a tungsten tip as a second electrode. Weight losses during the melting process were negligible. The product always contained a small amout of $In_3Ir_3B$.

$In_3Ir_3B$ and $In_3Rh_3B$ are formed as dark gray powders, $In_5Ir_9B_4$ as a gray regulus. All three compounds are stable to air and moisture, and even on treatment with concentrated hydrochloric acid no attack was observed. They are, however, rapidly decomposed by hot aqua regia.

## 2.2. Resistivity

The electrical resistance of a pressed and sintered $(900\,°C)$ powdered sample of $In_3Ir_3B$ was measured in the range of 4.2–293 K by applying a dc four-probe method.

## 2.3. Density measurements

The densities of powdered samples of $In_3Ir_3B$ and $In_3Rh_3B$ were measured pycnometrically at $25\,°C$ using monobromobenzene as a displacement liquid.

## 2.4. X-ray diffraction and crystal structure

For phase identification and for the determination of lattice constants at room temperature, X-ray powder methods were applied using a powder diffractometer (Stoe) and a Guinier-camera ($CuK\alpha_1$ radiation, quartz monochromator, Si as internal standard), respectively. For low temperatures a Huber Guinier-diffractometer ($CuK\alpha_1$ radiation) equipped with a closed cycle helium cryostat was used.

Needle shaped single crystals of $In_3Ir_3B$ were isolated from a sample with composition $In_5Ir_3B$ heated to $1150\,°C$ for 50 h. In the case of $In_3Rh_3B$ the formation of single crystals (also needle shaped) could be achieved by carrying out the synthesis with a compact piece of indium instead of indium powder. The crystals were first investigated on a

precession camera (Zr-filtered $MoK\alpha$ radiation). Several reciprocal lattice layers were recorded. Their inspection revealed hexagonal symmetry with the diffraction symbol $6/mmm P$- - -. Of the associated space groups $P\bar{6}2m$ turned out to be the right one in the course of the structure determination.

An irregular shaped single crystal of $In_5Ir_9B_4$ was obtained from the crushed regulus.

X-ray intensity data of $In_3Ir_3B$ and $In_3Rh_3B$ were collected using a four-circle diffractometer (CAD4, Enraf-Nonius, graphite-monochromated $MoK\alpha$ radiation, $\omega/2\theta$-mode). In the case of $In_5Ir_9B_4$, an image plate diffraction system (Stoe, IPDS2) was used. The structures of all three compounds were solved in space group $P\bar{6}2m$ by means of direct methods with SHELXS [17] and refined using SHELXL-97 [18] based on $F^2$. In the refinement of the isotypic compounds $In_3Ir_3B$ and $In_3Rh_3B$, anisotropic displacement parameters were used only for iridium and rhodium, respectively. In the first stages the indium atoms were placed on the Wykoff position $3g$ with point symmetry $mm$. However, the refinement resulted in extremely anisotropic thermal ellipsoids. As no superstructure reflections could be detected in the precession photographs, this gave rise to locating the indium atoms on two near-neighboring split positions (both with Wykoff position $6k$, point symmetry $m$) close to the $(1\bar{1}0)$ mirror plane. The occupation parameters of these positions were refined to about 0.4 for In1 and 0.1 for In2. The split positions as well as the boron atoms were refined considering isotropic displacement parameters. A subsequent difference Fourier synthesis revealed no significant residual peaks.

$In_5Ir_9B_4$ crystallizes in space group $P\bar{6}2m$, but the symmetry is close to $P6/mmm$. The structure was refined with anisotropic displacement parameters for indium and iridium. Again highly anisotropic thermal ellipsoids were found, especially for In3. They are discussed in Section 3. The refinement of In3 on a split position was not successful.

Crystallographic data and details concerning the data collection and the structure refinement are given in Table 1. Atomic coordinates, displacement parameters and selected interatomic distances are listed in Tables 2 and 3.

## 3. Results and discussion

### 3.1. $In_3Ir_3B$ and $In_3Rh_3B$

The structure of the isotypic compounds $In_3Ir_3B$ and $In_3Rh_3B$ is related to the $Fe_2P$ type. The indium and platinum metal atoms adopt the positions of the iron atoms in $Fe_2P$. One third of the positions of the P atoms are occupied by boron atoms while two thirds remain empty. The $In_3Ir_3B$ structure is shown as a projection along the hexagonal axis in Fig. 1. It is characterized by a three-dimensional framework of indium atoms in which columns of boron centered triangular iridium prisms connected by their triangular faces are inserted. The indium atoms are

Table 1
Crystallographic and data collection parameters

| Compound | $In_3Ir_3B$ | $In_3Rh_3B$ | $In_5Ir_9B_4$ |
|---|---|---|---|
| Crystal system | Hexagonal | Hexagonal | Hexagonal |
| Space group | $P\bar{6}2m$ | $P\bar{6}2m$ | $P\bar{6}2m$ |
| $a$, $b$ (pm) | 685.78(1) | 678.47(3) | 559.0(2) |
| $c$ (pm) | 287.30(1) | 288.61(6) | 1032.6(3) |
| Volume ($10^6$ pm$^3$) | 117.01(1) | 115.05(1) | 279.46(11) |
| $Z$ | 1 | 1 | 1 |
| Density (calculated/measured) (g/cm$^3$) | 13.23/13.19 | 9.58/9.51 | 13.95 |
| Applied radiation, $\lambda$ (pm) | Mo$K\alpha$, 710.73 | Mo$K\alpha$, 710.73 | Mo$K\alpha$, 710.73 |
| Absorption coefficient (mm$^{-1}$) | 99.30 | 25.09 | 112.27 |
| Crystal size (mm$^3$) | $0.002 \times 0.002 \times 0.1$ | $0.002 \times 0.002 \times 0.1$ | $0.03 \times 0.03 \times 0.03$ |
| Theta range for data collection | 3–45° | 3–40° | 3–30° |
| $h_{min}$, $h_{max}$, $k_{min}$, $k_{max}$, $l_{min}$, $l_{max}$ | −13,13,−13,13,0,5 | −12,12,−12,12,−5,5 | −7,7,−7,7,−14,14 |
| Reflections collected/unique/($I > 2\sigma(I)$) | 2171/396/374 | 2818/300/281 | 5463/326/310 |
| Absorption correction | Numerical | Numerical | Empirical, equival. |
| $R$(int) | 0.0497 | 0.0664 | 0.1303 |
| Number of variables | 15 | 15 | 22 |
| $R1(I > 2\sigma(I))$ | 0.0338 | 0.0388 | 0.0279 |
| $R1$ (all data) | 0.0380 | 0.0466 | 0.0306 |
| w$R2$ | 0.0861 | 0.1033 | 0.0515 |
| w$R2$ (all data) | 0.0888 | 0.1083 | 0.0531 |
| Goodness of fit on $F^2$ | 1.133 | 1.120 | 1.113 |
| Extinction coefficient | 0.053(5) | 0.143(15) | 0.0052(3) |
| Flack parameter | 0.01(4) | −0.1(3) | Inversion twin |
| Residual electron density/(e$^-$/Å$^3$) | −6.63/8.73 | −3.47/5.84 | −3.98/2.88 |
| Structure refinement program | SHELX97 (on $F^2$) | SHELX97 (on $F^2$) | SHELX97 (on $F^2$) |

Table 2
Positional parameters and anisotropic displacement parameters (pm$^2$, $U_{13} = U_{23} = 0$)

| Atom | Site | $x/a$ | $y/b$ | $z/c$ | Occup. | $U_{11}$ | $U_{22}$ | $U_{33}$ | $U_{12}$ |
|---|---|---|---|---|---|---|---|---|---|
| $In_3Rh_3B$ | | | | | | | | | |
| Rh | 3f | 0.2414(1) | 0 | 0 | 1 | 45(3) | 52(4) | 45(4) | 26(2) |
| In1 | 6k | 0.5983(3) | 0.0263(4) | 0.5 | 0.412(7) | 64(4) | | | |
| In2 | 6k | 0.6244(19) | 0.109(3) | 0.5 | 0.105(8) | 150(20) | | | |
| B | 1b | 0 | 0 | 0.5 | 1 | 90(40) | | | |
| $In_3Ir_3B$ | | | | | | | | | |
| Ir | 3f | 0.24311(8) | 0 | 0 | 1 | 48(2) | 61(2) | 69(2) | 30(1) |
| In1 | 6k | 0.5984(4) | 0.0246(6) | 0.5 | 0.366(8) | 87(5) | | | |
| In2 | 6k | 0.624(2) | 0.103(3) | 0.5 | 0.12(1) | 160(30) | | | |
| B | 1b | 0 | 0 | 0.5 | 1 | 40(30) | | | |
| $In_5Ir_9B_4$ | | | | | | | | | |
| Ir1 | 3f | 0.4870(3) | 0 | 0 | 1 | 66(4) | 96(3) | 73(4) | 33(2) |
| Ir2 | 6i | 0 | 0.4873(2) | 0.27645(6) | 1 | 63(3) | 116(3) | 78(3) | 31(2) |
| In1 | 2d | 1/3 | 2/3 | 0.5 | 1 | 127(5) | 127(5) | 77(8) | 64(3) |
| In2 | 2e | 0 | 0 | 0.3383(3) | 1 | 100(6) | 100(6) | 309(13) | 50(3) |
| In3 | 1a | 0 | 0 | 0 | 1 | 89(9) | 89(9) | 640(27) | 44(5) |
| B | 4h | 1/3 | 2/3 | 0.143(2) | 1 | 57(34) | | | |

The anisotropic thermal displacement factor takes the form: $\exp[-2\pi^2(h^2 a^{*2} U11 + k^2 b^{*2} U22 + \cdots + 2klb^*c^* U23)]$.

disordered. They are located on two near-neighboring split positions—the overlapping balls in Fig. 1—with occupation parameters close to 0.4 for In1 (dark gray balls in Fig. 1) and 0.1 for In2 (light gray balls) and distances In1–In1 = 30 pm, In2–In2 = 122 pm. That means that on average one indium atom is distributed over four near-neighboring positions, while locally only one of these four positions can be occupied.

The perspective view of Fig. 2 shows a column of boron atom centered triangular iridium prisms surrounded by interconnected triangular prisms of indium atoms which are shifted by $c/2$ relative to the iridium prisms. The shape of the indium prisms is irregular owing to the split positions. However, for simplicity only the centers of the In1/In2-groups are connected by straight lines in Fig. 2. The Ir–Ir distances of 287 and 289 pm (Rh: 284 and

Table 3
Selected interatomic distances (pm)

**In₃Rh₃B**

| Rh– | | | | B– | | | | In1– | | | | In2– | | | |
|---|---|---|---|---|---|---|---|---|---|---|---|---|---|---|---|
| | Rh | 2× | 283.7(2) | | Rh | 6× | 218.30(8) | | Rh | 2× | 274.7(1) | | Rh | 2× | 266.3(9) |
| | | 2× | 288.61(6) | | In1 | 2.4× | 281.9(1) | | | 2× | 276.8(1) | | | 2× | 273.1(9) |
| | In1 | 1.6× | 274.7(1) | | In2 | 0.6× | 298.8(11) | | | 2× | 292.2(2) | | | 2× | 328(1) |
| | | 1.6× | 276.8(1) | | | | | | In1[a] | 1.6× | 290.3(1) | | In1[a] | 0.8× | 293.0(3) |
| | | 1.6× | 292.2(2) | | | | | | In2[a] | 0.2× | 293.0(3) | | | 0.8× | 300.0(5) |
| | In2 | 0.4× | 266.3(9) | | | | | | | 0.2× | 300.0(5) | | In2[a] | 0.4× | 315.9(13) |
| | | 0.4× | 273.1(9) | | | | | | In1[b] | 3.2× | 328.1(4)–379.5(4) | | In1[b] | 3.2× | 283(2)–429(2) |
| | | 0.4× | 328(1) | | | | | | In2[b] | 0.8× | 283(2)–429(2) | | In2[b] | 0.4× | 339.7(1) |
| | B | 2× | 218.30(8) | | | | | | | | | | | 0.4× | 369.4(9) |
| | | | | | | | | | B | 1× | 281.9(1) | | B | 1× | 298.8(11) |

**In₃Ir₃B**

| Ir– | | | | B– | | | | In1– | | | | In2– | | | |
|---|---|---|---|---|---|---|---|---|---|---|---|---|---|---|---|
| | Ir | 2× | 287.30(1) | | Ir | 6× | 220.07(4) | | Ir | 2× | 276.0(2) | | Ir | 2× | 267.3(10) |
| | | 2× | 288.77(9) | | In1 | 2.4× | 284.2(2) | | | 2× | 278.7(2) | | | 2× | 274.9(10) |
| | In1 | 1.6× | 276.0(2) | | In2 | 0.6× | 299.0(12) | | | 2× | 293.4(2) | | | 2× | 326.5(13) |
| | | 1.6× | 278.7(2) | | | | | | In1[a] | 1.6× | 288.78(7) | | In1[a] | 0.8× | 291.2(3) |
| | | 1.6× | 293.4(2) | | | | | | In2[a] | 0.2× | 291.2(3) | | | 0.8× | 297.2(5) |
| | In2 | 0.4× | 267.3(10) | | | | | | | 0.2× | 297.2(5) | | In2[a] | 0.4× | 312.1(12) |
| | | 0.4× | 274.9(10) | | | | | | In1[b] | 3.2× | 333.7(6)–382.1(6) | | In1[b] | 3.2× | 297.2(5)–408.0(5) |
| | | 0.4× | 326.5(13) | | | | | | In2[b] | 0.8× | 297.2(5)–408.0(5) | | In2[b] | 0.4× | 343.9(2) |
| | B | 2× | 220.07(4) | | | | | | | | | | | 0.4× | 373.4(10) |
| | | | | | | | | | B | 1× | 284.2(2) | | B | 1× | 299.0(12) |

**In₅Ir₉B₄**

| Ir1– | | | | Ir2– | | | | In1– | | | | In2– | | | |
|---|---|---|---|---|---|---|---|---|---|---|---|---|---|---|---|
| | Ir1 | 4× | 279.8(1) | | Ir1 | 1× | 285.5(1) | | Ir2 | 6× | 281.74(8) | | Ir2 | 3× | 279.8(2) |
| | Ir2 | 2× | 285.5(1) | | Ir2 | 2× | 279.8(1) | | In1 | 3× | 322.7(1) | | | 3× | 293.6(2) |
| | In3 | 1× | 286.7(2) | | In1 | 2× | 281.74(8) | | In2 | 6× | 363.4(2) | | In1 | 6× | 363.4(2) |
| | B | 4× | 219.1(13) | | In2 | 1× | 279.8(2) | In3– | Ir1 | 3× | 272.3(2) | | In2 | 1× | 334.0(5) |
| B– | Ir1 | 3× | 219.1(13) | | | 1× | 293.6(2) | | | 3× | 286.7(2) | | In3 | 1× | 349.3(3) |
| | Ir2 | 3× | 212.1(12) | | B | 2× | 212.1(12) | | In2 | 2× | 349.3(3) | | | | |

[a] Distances in *c*-direction.
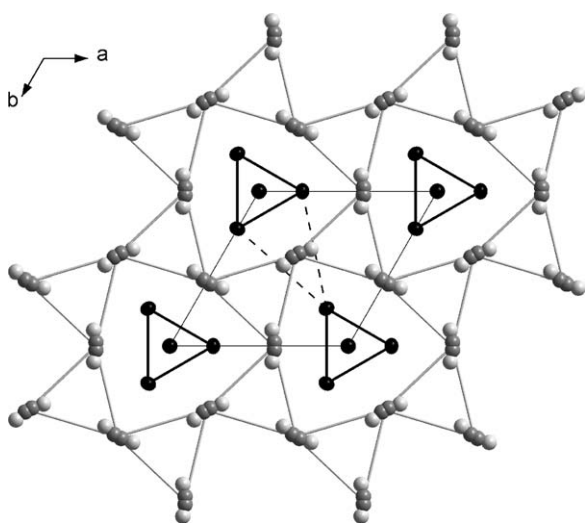[b] Distances in the *a/b* plane.



Fig. 1. Structure of In₃Ir₃B (Fe₂P derivative structure), projection along [001]. Large black balls: Ir at $z = 0$; small black balls: B at $z = 1/2$. Indium on split positions: In1(occupation parameter ∼0.4), dark gray at $z = 1/2$; In2 (occupation parameter ∼0.1), light gray at $z = 1/2$. Lines between atoms denote triangular prisms as building elements, they do not necessarily represent the strongest bonds. This holds for all figures.
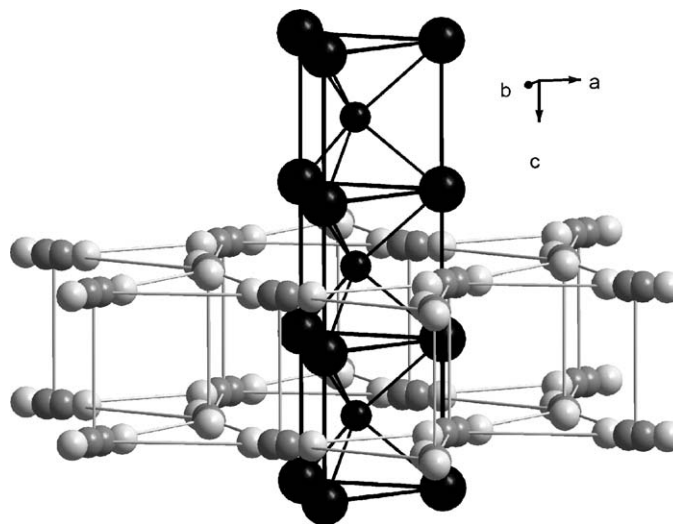


Fig. 2. Section of the In₃Ir₃B structure showing a column of boron centered triangular iridium prisms (black balls) surrounded by interconnected triangular prisms of indium atoms (lines connect only the centers of the split positions) shifted by $c/2$ relative to the iridium prisms.

289 pm) are slightly larger than in iridium metal (271.5 pm, Rh: 269.0 pm [19]), while the Ir–B distance of 220 pm (Rh–B: 218 pm) is slightly larger than the sum of the covalent radii (209 pm, Rh–B: 207 pm [27]). These distances are in the upper region of what is usually found in metal-rich ternary borides of iridium and rhodium. Similar distances are found in $ZnIr_4B_3$ [20]: $d$(Ir–Ir) = 280 and 294 pm; $d$(Ir–B) = 215–219 pm.

The indium atoms are located in front of the rectangular faces and in front of the edges of the iridium prisms. The Ir–In distances for the face capping indium atom are 279 and 293 pm (Rh: 277 and 292 pm) if one of the In1 positions is occupied, and 267 and 327 pm (Rh: 266 and 328 pm) if one of the In2 positions is occupied. The Ir–In distances for the edge capping indium atom are 276 pm in the case of In1 (Rh: 275 pm) and 275 pm in the case of In2 (Rh: 273 pm). All these distances are within the range of In–Ir distances found in comparable compounds like $In_2Ir$ [21] (270–286 pm) or $In_3Ir$ [22] (253–326 pm). As a whole the iridium atoms have coordination number 12 (2B, 4Ir, 6In). The environment of the boron atoms is confined to the six iridium atoms of the triangular prism. The distance to the indium atoms in front of the prism faces (284 pm, Rh: 282 pm) is much longer than the sum of the metallic radii (264 pm). Therefore no bonding interactions are to be expected.

The indium atoms have six iridium and six indium neighbors. Four indium neighbors are in the hexagonal plane (see Fig. 1). The distances to them vary in the range from 297 to 408 pm (Rh: 283–429 pm), depending on their specific location in the system of split positions. The shortest distance between two In2 positions (250 pm) is hereby excluded because they cannot be occupied simultaneously. Before discussing the two indium neighbors in $c$ direction we will look at the arrangement of the iridium neighbors. As outlined in Fig. 1 by the broken lines and shown in detail in Fig. 3, the iridium neighbors are located at the corners of a laterally stretched triangular prism which is formed between two Ir/B columns. In c-direction these prisms pile up to a column (Fig. 3). The indium atoms are shifted away from the middle of the prisms according to their distribution over the split positions. If they were exactly in the middle of the prisms, they would form a linear chain with an intrachain distance of 287.3 pm (Rh: 288.6 pm), corresponding to the lattice constant c, which is very short. In the structure of the element the In–In distances are 324.8 and 337.6 pm [31], and this is also the range in which most of the In–In distances in intermetallic compounds of indium are to be found. However, In–In distances shorter than 290 pm have indeed been reported for several compounds (examples are $La_4Pd_{10}In_{21}$ [23]: 285.8 and 288.6 pm; $Gd_3Pt_4In_{12}$ [24]: 284.3 pm; $EuRh_2In_8$ [25]: 288.1 and 289.5 pm; $La_3In_4Ge$ [26]: 286.6 pm). Nevertheless such short distances can be considered as stressed, and it is supposed that they are avoided if possible. In the case of the $In_3Ir_3B$ structure this is most probably achieved by forming an indium zig-zag chain inside the column of
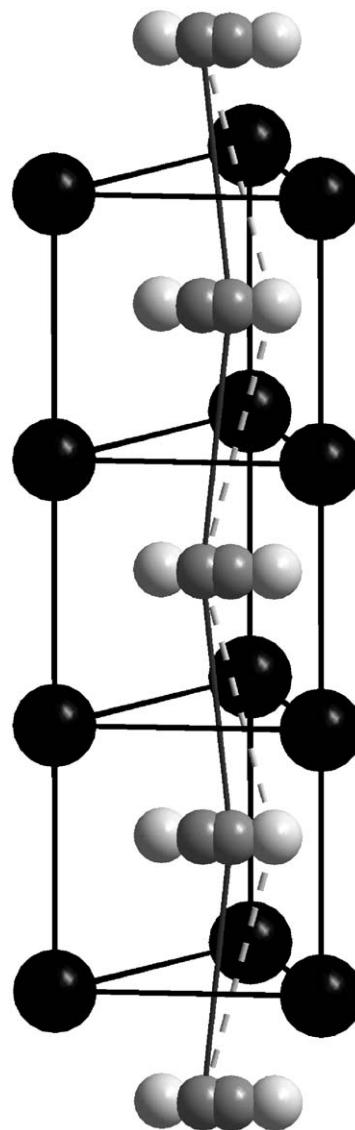


Fig. 3. Section of the $In_3Ir_3B$ structure showing a column of laterally stretched triangular iridium prisms (black balls; outlined by dotted lines in Fig. 1). Lines between indium atoms (dark gray: split position In1, light gray: split position In2) denote the supposed formation of disordered zig-zag chains (see text).

triangular iridium prisms as indicated in Fig. 3. This results in a slightly enlarged distance of 288.8 pm (Rh: 290.3 pm) if only the In1 positions are occupied, which holds for 80% of the indium atoms. The distance rises to 297 pm (Rh: 300 pm) if In1 and In2 positions alternate in successive prisms (dotted lines in Fig. 3). In an ordered structure the zig-zag chains would require a doubling of the lattice constant $c$. However, as stated in Section 2.4, no corresponding reflections could be detected in the precession photographs. Therefore the chains must be disordered or ordered in domains too small to give rise to superstructure reflections. As an alternative to a static disorder there is also the possibility of a dynamic change between the split positions. A hint to such a dynamic process is provided by the temperature dependence of the resistivity,
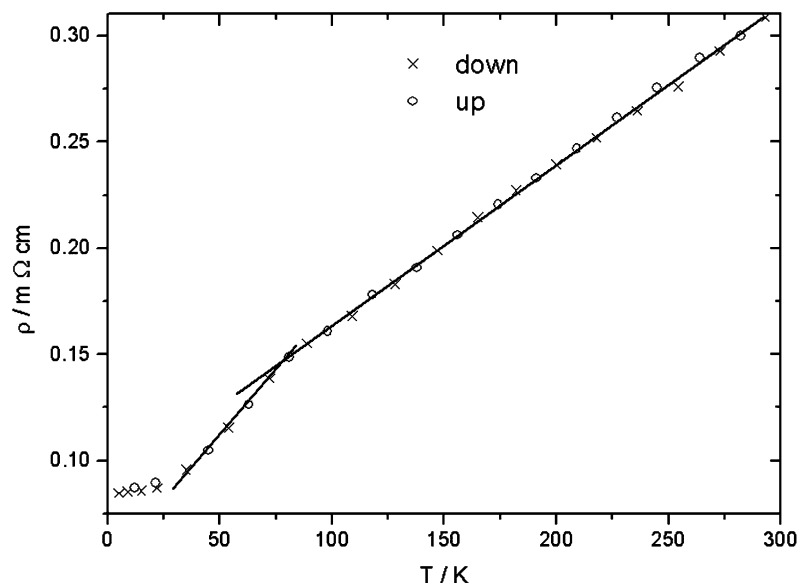
Fig. 4. Resistivity Versus temperature for a pressed and sintered powder sample of $In_3Ir_3B$ (four probe dc method) measured on cooling (crosses) and on warming (circles).



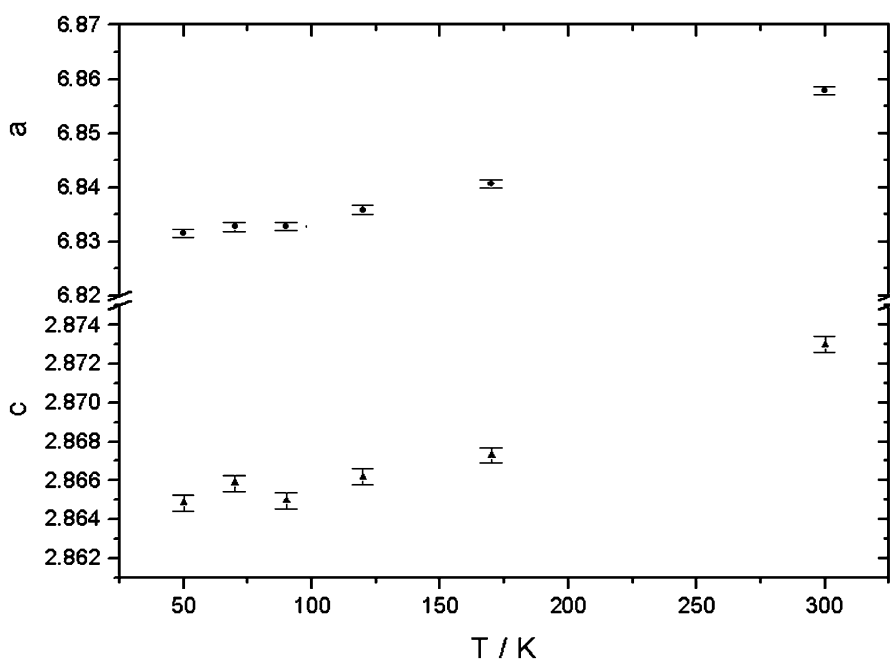Fig. 5. Lattice constants $a$ and $c$ (Å) Versus temperature for $In_3Ir_3B$ (Guinier powder diffractometer measurements).

which is shown for $In_3Ir_3B$ in Fig. 4. As expected for a metallic conductor the resistivity decreases linearly with decreasing temperature. However, at about 80 K the slope of the curve changes and a second linear $\rho(T)$ region is observed until below about 30 K the residual resistivity becomes dominating. This is an indication of a phase transition around 80 K. Therefore X-ray powder diagrams were recorded above and below the transition temperature. As they did not show any visible differences, a change of the structure type can be excluded. The graphs of lattice

constants versus temperature calculated from these powder diagrams are shown in Fig. 5. Particularly from the $a(T)$ graph a considerable reduction in thermal expansion below a temperature around 80 K is apparent. In spite of the fact that for metals a decrease of the linear thermal expansion coefficient with decreasing temperature is frequently observed, this may be taken as an additional indication of a phase transition. Since a drastic structural change can be excluded, this transition may possibly be attributed to a change from dynamic to static disorder of the indium atoms.
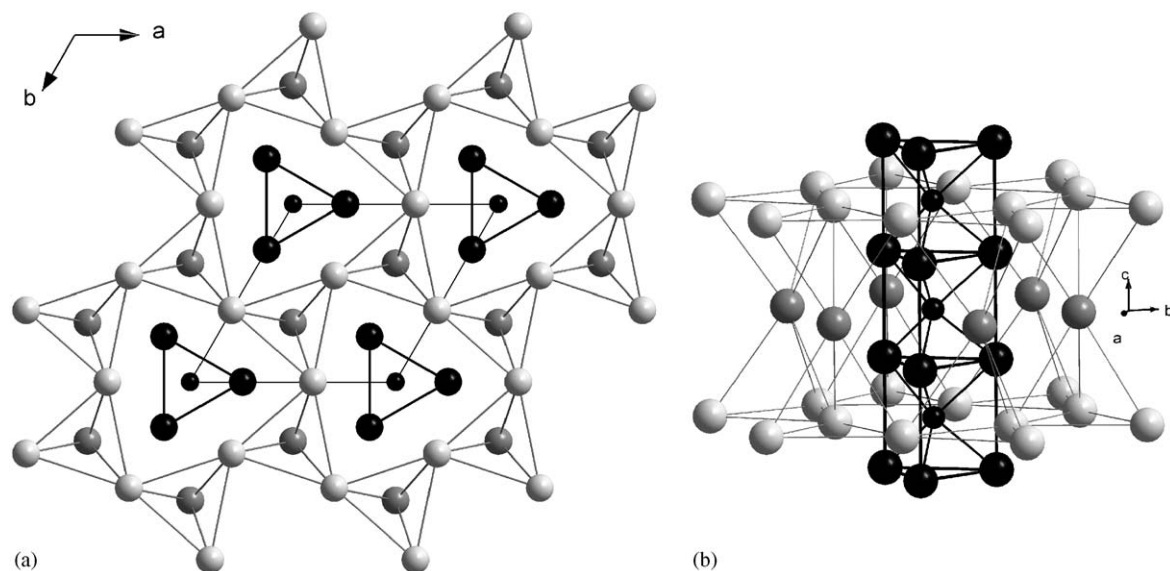
Fig. 6. Structure of $Sn_5Ir_6B_2$ ($P\bar{6}2m$; $a = 659.0$ pm, $c = 559.2$ pm; $Fe_2P$ derivative structure, large black balls: Ir at $z\sim1/4$ and $z\sim3/4$; small black balls: B at $z = 0$ and $z = 1/2$; light gray: Sn at $z = 0$; dark gray: Sn at $z = 1/2$.) (a) Projection along [001], and (b) perspective view of a section of the structure corresponding to that of $In_3Ir_3B$ depicted in Fig. 2.

The only structural relationship between the $In_3Ir_3B$ structure and the structures typical of the majority of ternary transition metal borides with aluminum and gallium as outlined in part 1 is provided by the boron centered triangular transition metal prism as a common building element. The topologies of the structures are completely different. We do not find In atoms in distorted cubes. Instead In–In contacts are dominating, and the coordination by transition metal atoms is reduced to the laterally stretched triangular prism described above. The main reason for this is probably the size of the indium atom. While aluminum and gallium atoms are of nearly equal size and small enough to fit into a transition metal cube without breaking the bonds between the transition metal atoms, the indium atoms are much larger. They are comparable in size to tin atoms (metallic radii for CN 12 [27]: Al 143 pm, Ga 141 pm, In 166 pm, Sn 162 pm). It is hardly surprising then that the structure of $In_3Ir_3B$ is similar to the structure of a tin iridium boride. For comparison the structure of $Sn_5Ir_6B_2$ [28], which is also related to the $Fe_2P$ type, is shown as a projection in Fig. 6a. The difference is that the tin prisms surrounding an Ir/B column are twice as long as the $Ir_6B$ prisms and that they are centered by an additional tin atom (Fig. 6b). This results in the formation of tin tetrahedra and doubling of the lattice constant c compared to the $In_3Ir_3B$ structure.

### 3.2. $In_5Ir_9B_4$

The structure of $In_5Ir_9B_4$ is shown as a projection along [001] in Fig. 7. It may be derived from the $CeCo_3B_2$ type [29], which is a ternary variant of the $CaCu_5$ type structure [30]. In the structure of $CeCo_3B_2$, the cobalt atoms are arranged in kagomé nets perpendicular to the c-axis. By
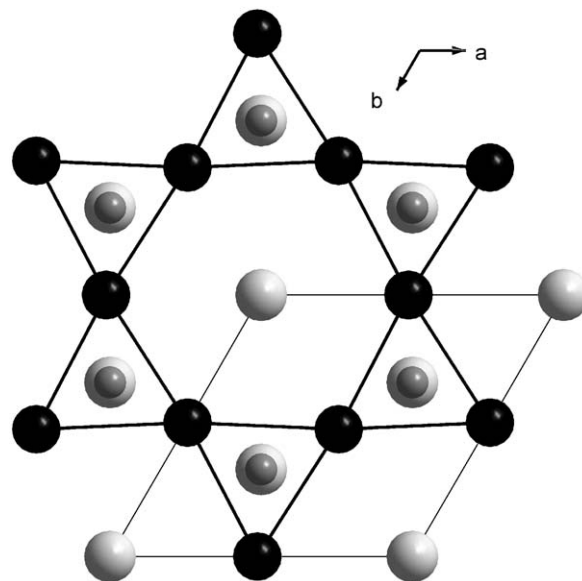


Fig. 7. Structure of $In_5Ir_9B_4$ ($CeCo_3B_2$ derivative structure), projection along [001]. Large black balls: Ir; small gray balls: B; large gray balls: In.

stacking these nets hexagonal channels are formed, surrounded by six columns of triangular prisms which are centered by the boron atoms. The cerium atoms in the channels are at the same height as the boron atoms and thus they are coordinated by 12 cobalt atoms forming a hexagonal prism.

In the $In_5Ir_9B_4$ structure the kagomé nets, which are slightly distorted in this case, are formed by the iridium atoms. We arrive at the composition $In_5Ir_9B_4$ if we take the formula $InIr_3B_2$ three times and replace two boron atoms by indium atoms (In1 in the structure). As shown in the
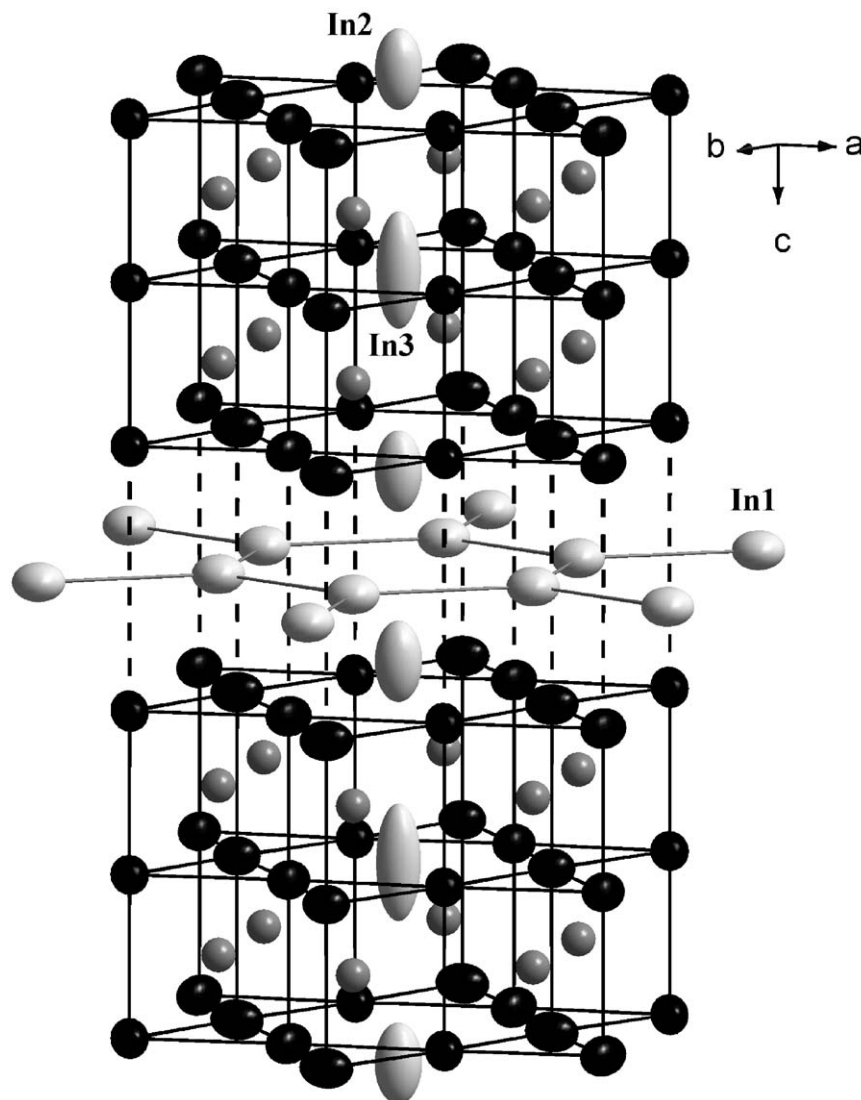
Fig. 8. Perspective view of the $In_5Ir_9B_4$ structure. The atoms are represented by their thermal ellipsoids (black: Ir, dark gray: B, light gray: In). The dotted lines denote long Ir–Ir distances of 462 pm in triangular Ir prisms stretched in $c$-direction. For the extremely anisotropic thermal ellipsoids of the In atoms in the channel see text.

perspective view of Fig. 8, in which the atoms are represented by their thermal ellipsoids, these indium atoms (In1) are located at the centers of triangular iridium prisms elongated in $c$-direction. The dotted lines in Fig. 8 represent large Ir–Ir distances of 462 pm. Therefore the structure can be seen as a layer structure in which slabs formed by double layers of triangular $Ir_6B$ prisms are separated by honeycomb nets (Schlaefli symbol $6^3$) of In1 atoms. But from Figs. 7 and 8 it is evident that the structure can also be seen as a channel structure. The indium atoms In2 and In3 form a linear chain inside of a channel with hexagonal cross-section. Deviating from the $CeCo_3B_2$ structure, they are not at the height of the boron atoms. In2 is situated between an indium $6^3$ net and the outer kagomé net of an Ir/B slab while In3 centers the hexagon of the kagomé net in the middle of the Ir/B slab. However, as can be seen from Fig. 8, their thermal

ellipsoids, especially those of the In3 atoms, are extremely anisotropic. The reason is probably that the In3 atoms in reality are shifted to positions just above or below the kagomé net in order to optimize the distances to their neighboring atoms. The refinement of In3 on a split position, however, was not successful. There is possibly a dynamic change between these near-neighboring positions. The elongation of the In2 ellipsoid may be due to smaller shifts along $c$ as a consequence of the In3-shifts. The distances between the indium atoms in the channels are 334 pm (In2–In2) and 349 pm (In2–In3). Those in the $6^3$ net are 323 pm (In1–In1), and those between In2 and In1 (363 pm) are so long that no bonding interactions need be assumed. The Ir–Ir distances of 280 and 286 pm are close to those found in the structure of $In_3Ir_3B$. The boron atoms are not exactly in the centers of the triangular iridium prisms. They are shifted in $c$-direction towards the outer

kagomé nets (Ir2) of the Ir/B slab. Therefore they have three near Ir neighbors (Ir2) at a distance of 212 pm and three more distant ones with 219 pm. Ir–In distances are in the range of 280–293 pm.

## References

[1] H.J. Becher, K. Krogmann, E. Peisker, Z. Anorg. Allg. Chem. 344 (1966) 140–147.

[2] Yu.B. Kuz'ma, N.F. Chaban, Izvest. Akad. Nauk. SSSR, Neorg. Mat. 5 (1969) 384–385.

[3] W. Jeitschko, Acta Cryst. B 25 (1969) 163–164.

[4] Yu.B. Kuz'ma, N.F. Chaban, Izvest. Akad. Nauk. SSSR, Neorg. Mat. 9 (1973) 1908–1911.

[5] K. Schweitzer, W. Jung, Z. Kristallogr. 174 (1986) 109–110.

[6] W. Jung, K. Petry, Z. Kristallogr. 182 (1988) 153–154.

[7] H. Hartung, W. Jung, to be published.

[8] K. Petry, W. Kluenter, W. Jung, Z. Kristallogr. 209 (1994) 151–156.

[9] N.F. Chaban, Yu.B. Kuz'ma, Dopov. Akad. Nauk Ukr. RSR, Ser. A 6 (1973) 550.

[10] M.-L. Fiedler, H.H. Stadelmaier, E.B. Snipes, Z. Metallkd 68 (1977) 765.

[11] H.H. Stadelmaier, M.-L. Fiedler, Z. Metallkd. 60 (1969) 447.

[12] W. Kluenter, W. Jung, Z. Anorg. Allg. Chem. 621 (1995) 197–200.

[13] E. Ganglberger, H. Nowotny, F. Benesovsky, Mh. Chem. 96 (1965) 1144.

[14] T. Adelsberger, M. Jansen, Z. Anorg. Allg. Chem. 625 (1999) 438.

[15] H. Holleck, J. Less Common Met. 52 (1977) 167.

[16] J.-D. Schoebel, H.H. Stadelmaier, Z. Metallkd. 55 (1964) 378.

[17] G.M. Sheldrick, SHELXS, Programm zur Kristallstrukturlösung, University Göttingen, 1990.

[18] G.M. Sheldrick, SHELXL-97, Programm zur Kristallstrukturlösung, University Göttingen, 1997.

[19] E.A. Owen, E.L. Yates, Phil. Mag. 15 (1933) 472–488.

[20] K. Petry, W. Jung, J. Alloys Compd. 183 (1992) 363–376.

[21] M.F. Zumdick, G.A. Landrum, R. Dronskowski, R.-D. Hoffmann, R. Poettgen, J. Solid State Chem. 150 (2000) 1–19.

[22] R. Poettgen, R.-D. Hoffmann, G. Kotzyba, Z. Anorg. Allg. Chem. 624 (1998) 244–250.

[23] V.I. Zaremba, U.C. Rodewald, Ya.M. Kalychak, Ya.V. Galadzhun, D. Kaczorowski, R.-D. Hoffmann, R. Poettgen, Z. Anorg. Allg. Chem. 629 (2002) 434–442.

[24] U.C. Rodewald, V.I. Zaremba, Ya.V. Galadzhun, R.-D. Hoffmann, R. Poettgen, Z. Anorg. Allg. Chem. 628 (2002) 2293–2298.

[25] R. Poettgen, D. Kussmann, Z. Anorg. Allg. Chem. 627 (2001) 55–60.

[26] A.M. Guloy, J.D. Corbett, Inorg. Chem. 35 (1996) 2616–2622.

[27] L. Pauling, Die Natur der Chemischen Bindung, Verlag Chemie, Weinheim, 1973.

[28] W. Kluenter, W. Jung, Z. Anorg. Allg. Chem. 622 (1996) 2099–2106.

[29] Yu.B. Kuz'ma, P.I. Kripyakevich, N.S. Bilonizhko, Dopov. Akad. Nauk Ukr. RSR Ser. A 31 (1969) 939–941.

[30] W. Haucke, Z. Anorg. Allg. Chem. 244 (1940) 17–22.

[31] J. Graham, A. Moore, G.V. Raynor, Z. Anorg. Allg. Chem. 286 (1956) 118–135.